The Skin-Layer Ocean Heat Flux Instrument (SOHFI). Part II: Field Measurements of Surface Heat Flux and Solar Irradiance

L. A. SROMOVSKY, J. R. ANDERSON, F. A. BEST, J. P. BOYLE, C. A. SISKO, AND V. E. SUOMI*

Space Science and Engineering Center, University of Wisconsin—Madison, Madison, Wisconsin

(Manuscript received 31 March 1998, in final form 13 November 1998)

ABSTRACT

The Skin-Layer Ocean Heat Flux Instrument (SOHFI) described by Sromovsky et al. (Part I, this issue) was field-tested in a combination of freshwater and ocean deployments. Solar irradiance monitoring and field calibration techniques were demonstrated by comparison with independent measurements. Tracking of solar irradiance diurnal variations appears to be accurate to within about 5% of full scale. Preliminary field tests of the SOHFI have shown reasonably close agreement with bulk aerodynamic heat flux estimates in freshwater and ocean environments (generally within about 20%) under low to moderate wind conditions. Performance under heavy weather suggests a need to develop better methods of submergence filtering. Ocean deployments and recoveries of drifting SOHFI-equipped buoys were made during May and June 1995, during the Combined Sensor Program of 1996 in the western tropical Pacific region, and in the Greenland Sea in May 1997. The Gulf Stream and Greenland Sea deployments pointed out the need for design modifications to improve resistance to seabird attacks. Better estimates of performance and limitations of this device require extended intercomparison tests under field conditions.

1. Introduction

The design and basic operation of the Skin-Layer Ocean Heat Flux Instrument (SOHFI) is described by Sromovsky et al. (1999), hereafter referred to as Part I. In brief, the instrument uses heat flux sensors positioned within the skin layer where transport is through either conduction or radiation. Two sensors of differing solar sensitivity are used to separate solar irradiance from conducted heat fluxes. Following laboratory verification of SOHFI's heat flux measurement performance, we conducted field tests to determine the impact of natural wind and wave conditions, as well as other unanticipated environmental factors. Here we present the results of our preliminary field tests, followed by an assessment of the current state of SOHFI development and performance. Initial tests were in freshwater, primarily for convenience of instrument access and availability of ancillary measurements. To date, the most serious limitations of the instrument are susceptibility to seabird attacks and uncertain performance under severe weather conditions.

* Deceased.

Corresponding author address: Dr. L. A. Sromovsky, Space Science and Engineering Center, University of Wisconsin—Madison, 1225 West Dayton Street, Madison, WI 53706.
E-mail: larry.sromovsky@ssec.wisc.edu

2. Freshwater field tests

Two field tests in freshwater lakes provided limited confirmation of heat flux and solar irradiance measurements under field conditions.

a. Bulk aerodynamic comparisons at Sparkling Lake

These tests investigated whether winds and waves might produce skin depth variations or flux plate displacements from the surface that would lead to substantial measurement errors. The results of the analysis described below provide significant evidence of proper operation of the flux sensor under field conditions.

1) TEST CONFIGURATION

From July to November 1993, heat flux sensors were deployed from a raft located near the center of Sparkling Lake in northern Wisconsin. This small 20–m-deep lake is oblong in shape, with its longest dimension in the north–south direction. It is about 400 m wide at its midpoint and about 500–530 m wide over most of its 1200-m length. It is located about 2 km west and 6 km north of a nearby airport at which a meteorological data collection package was located. We chose this lake because of the instrumented raft already maintained on the lake as part of the National Science Foundation's (NSF's) Long-Term Ecological Research Program. The raft was anchored near the lake's center and equipped

to measure the wind speed at 1, 2, and 3 m above the surface, the atmospheric and wet-bulb temperatures at 2 m above the surface, and the water temperature at various levels under the raft. A shack on the raft housed the recording equipment. Measurements of downward longwave radiation (using an Eppley Precision Infrared Radiometer Model PIR) and downward solar radiation (using an Eppley Precision Spectral Pyranometer Model PSP) were obtained from a data collection package maintained at an airport 6 km south and 2 km east of the lake. These supporting measurements allowed us to make crude estimates of heat loss from the lake using bulk aerodynamic methods, which we could then compare with the flux plate measurements. The flux plate used during these tests had an aluminized Mylar film bonded on both sides of the standard flux plate to reflect solar radiation and thus minimize the solar heating of the flux plate.

Given the small size of Sparkling Lake, the use of bulk aerodynamic formulas are certainly questionable. However, according to Rao et al. (1974), for large fetch x, the equilibrium layer height h (the level at which the shear stress adjustment is at 90%) is approximately $x/200$, and the internal boundary layer thickness δ is about $x/100$. With the raft positioned in the middle of the lake and the fetch varying from about 200 to 600 m, depending on wind direction, this approximation yields $\delta = 2$–6 m, and $h = 1$–3 m. Thus, our atmospheric measurements at 2 m were most of the time within the internal boundary layer, and often within the equilibrium layer as well. Nevertheless, this is a marginal situation that could lead to the observed differences between SOHFI measurements and the bulk aerodynamic estimates, as discussed in subsequent sections.

Although we obtained encouraging results from these tests, they have considerable scatter that is understandable considering the following problems with the test conditions and supporting observations: 1) the longwave flux and solar flux observations are made over 6 km from the lake and thus may introduce both systematic and random errors, 2) the wind observations made on the lake have a good chance of being perturbed by the presence of the 2-m-high equipment shack on the raft, and 3) the shack could also produce wind shading and sun shading in certain configurations.

2) Flux analysis procedure

We compared SOHFI measurements with fluxes computed from the bulk aerodynamic equations. Following Kraus (1972), Fleagle and Businger (1980), or Guymer et al. (1983), the equations for heat and momentum fluxes can be written in the following form:

$$H_S = \rho_a C_S C_P U(T_s - \theta) \tag{1}$$

$$H_E = \rho_a C_E L U(q_s - q) \tag{2}$$

$$\tau = \rho_a C_D U^2, \tag{3}$$

where H_S and H_E are the sensible heat and evaporative heat transfers from the ocean to the atmosphere; τ is the surface wind stress; T_s is the surface temperature; $\theta = T + 0.0098z$ is the potential temperature at the reference level z; q_s and q are specific humidities (kg of water vapor per kg of air) at surface and reference levels, respectively; ρ_a is the density of air; C_p is the specific heat at constant pressure; L is the heat of vaporization; and U is the mean wind speed at the reference level measured relative to the surface current. The dimensionless bulk aerodynamic transfer coefficients are C_S for sensible heat, C_E for evaporative flux, and C_D for wind stress. All three of these coefficients depend on wind speed and stability, as discussed below. We approximated the net thermal radiation loss from the surface using

$$H_R = \epsilon(\sigma T_s^4 - H_{\mathrm{LW}}), \tag{4}$$

where H_{LW} denotes the incident downwelling longwave radiation, ϵ is the effective emissivity of the surface, T_s is the surface temperature, and σ is the Stefan–Boltzmann constant.

To evaluate the transfer coefficients, we used a relatively simple formulation provided by Kondo (1975). He approximated neutral stability transfer coefficients by simple polynomial functions of wind speed at the reference level, with results shown in Fig. 1a. His stability corrections are expressed in terms of a stability parameter S defined by

$$S = \frac{S_0|S_0|}{(|S_0| + 0.01)} \quad \text{and} \tag{5}$$

$$S_0 = [(T_s - \theta) + 0.61\theta(q_s - q)]U^{-2} \times [1 + \log 10/z]^{-2}, \tag{6}$$

in which the logarithm is base 10, z is in meters, U is in meters per second, and the temperature difference is adjusted to account for the buoyancy effects of water vapor (making the first bracketed term a virtual temperature difference). This stability parameter is similar to the bulk Richardson number (Stull 1988, p. 176), which we can approximate using

$$\mathrm{Ri} = -(gz/T_s)[(T_s - \theta) + 0.61\theta(q_s - q)]U^{-2}. \tag{7}$$

Kondo provided the following equations for the ratios of diabatic transfer coefficients to the neutral coefficients:

$$C_D/C_{ND} \approx C_S/C_{NS} \approx C_E/C_{NE} \approx 0 \quad \text{for } S \leq -3.3, \tag{8}$$

$$\approx 0.1 + 0.03S + 0.9\exp(4.8S) \quad \text{for } -3.3 < S < 0, \tag{9}$$

and, for unstable conditions ($S > 0$),

$$C_D/C_{ND} \approx 1 + 0.47S^{0.5} \quad \text{and} \tag{10}$$

$$C_S/C_{NS} \approx C_E/C_{NE} \approx 1 + 0.63S^{0.5}. \tag{11}$$

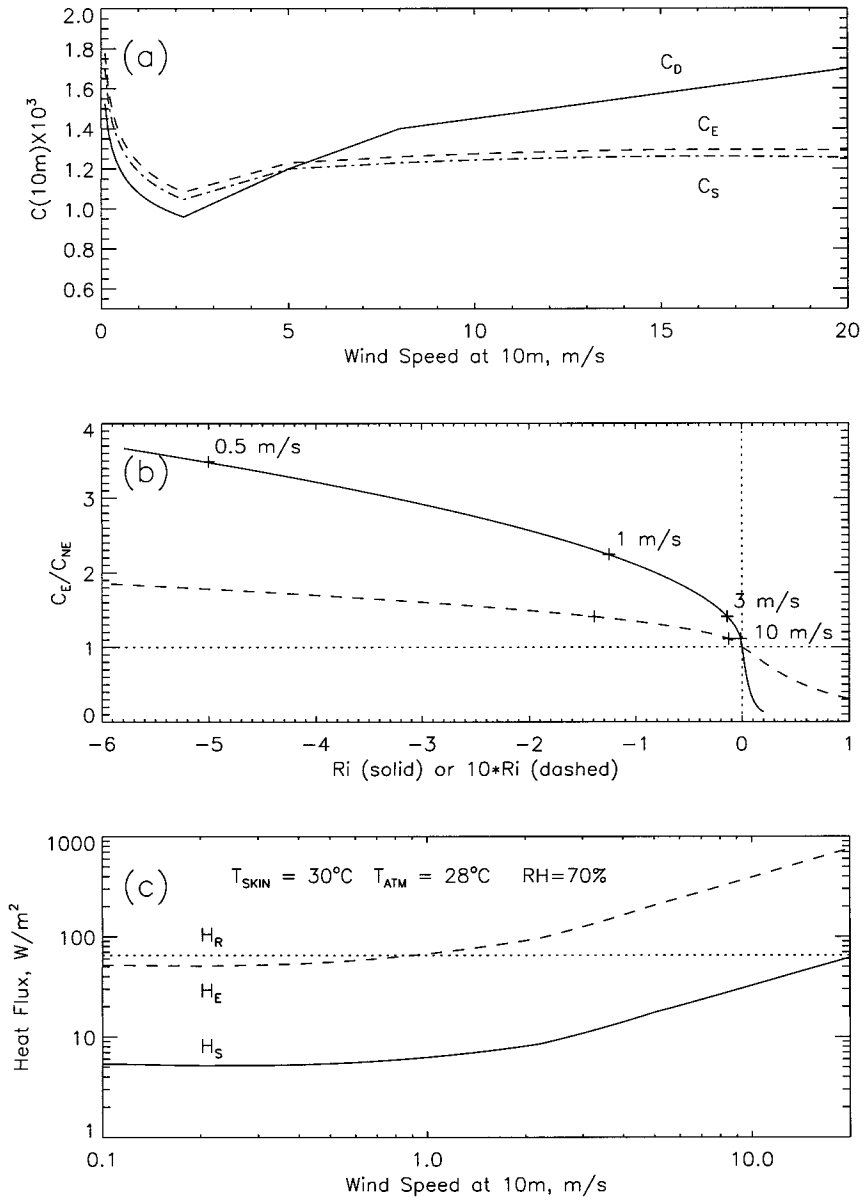

FIG. 1. Dependence of bulk aerodynamic transfer on wind speed and stability: (a) neutral stability transfer coefficients at 10 m as a function of wind speed at 10 m, (b) ratio of evaporative heat flux to the evaporative heat flux for neutral conditions vs Richardson number, and (c) evaporative and sensible heat fluxes for typical tropical Pacific conditions. the wind speed tick marks on the curves in (b) are for conditions given in (c).

The ratio for heat transport coefficients at $z = 10$ m is shown as a function of Richardson number in Fig. 1b. It is noteworthy that corrections increase dramatically for highly unstable conditions seen most often at low wind speeds (note the U^{-2} dependence in S and Ri). Figure 1c displays sample bulk aerodynamic fluxes for typical tropical Pacific conditions as a function of wind speed. Also shown is a typical net radiative flux under these conditions. Note the dominance of evaporative heat flux for wind speeds greater than a few meters per second.

The specific humidity at the surface was calculated assuming saturated air at the skin temperature, as measured by the thermocouple attached to the heat flux sensor. The specific humidity at 2 m was computed from the wet-bulb and dry-bulb temperatures using standard formulas, for example, the Smithsonian Meteorological Tables (List 1963). For the Sparkling Lake observations, we also adjusted the heat transfer coefficients from the 10-m standard level to the 2-m level using an iterative procedure described by Kondo (1975).

The temperature and wind measurements from day

195 to day 210 are shown in Fig. 2a. This period was characterized by significant diurnal variations in temperature and wind speed, with generally low dewpoint temperatures and a relatively warm lake, ensuring that evaporative heat transport would be the major contributor (Fig. 2b). The downward solar flux measurements, and our solar irradiance clear-sky model results are shown in Fig. 2c. The clear-sky solar flux model accounts for solar zenith angle and attenuation for an effective optical depth of 0.15. Also plotted is the difference between the SOHFI measured heat loss from the surface, H_{SOHFI}, and the bulk aerodynamic estimate, $H_{\mathrm{BULK}} = H_E + H_S + H_R$, scaled by a factor of 4 to facilitate comparison with the solar flux. It is evident, from the strong correlation between $H_{\mathrm{SOHFI}} - H_{\mathrm{BULK}}$ and the measured solar flux, that the SOHFI sensor responded significantly to sunlight, a characteristic that must be accounted for in our subsequent analysis.

3) Results for nighttime fluxes

To avoid the need for solar irradiance corrections and to restrain the extent of diabatic corrections, we first filtered the observations to exclude measurements made when solar fluxes exceeded 5 W m^{-2} or C_E/C_{EN} exceeded 1.5. The filtered time series SOHFI results from days 195–210 of 1993 are shown in Fig. 3, in comparison with the bulk aerodynamic results. The spike near day 201 and the increase from day 209 to day 210 are both correlated with sudden changes in evaporative heat loss when radiative losses were only slowly varying. On the other hand, the declining losses from day 196 to day 199 and the small peak near day 207 coincide with comparable IR flux variations (Fig. 2b). Clearly, the SOHFI measurements track many of the features seen in the bulk aerodynamic estimates, at both longer and shorter timescales. However, there appears to be a systematic difference between the two methods of heat flux measurement. The correlation plot in Fig. 3b seems to suggest an offset in the SOHFI measurements. This might be an indication of free convection effects playing a role at very low wind speeds; Bradley et al. (1991) for example, measured fluxes of 25 W m^{-2} under zero mean wind conditions. However, our filtering of the data should remove cases requiring strong diabatic corrections. Furthermore, the observations can be fit just as well without an offset, if we allow a calibration error in the SOHFI measurement system or a rescaling of the bulk aerodynamic coefficients, in which the latter is possibly justified on the basis of the small size of Sparkling Lake. Although they filtered the data somewhat differently, Suomi et al. (1996) found a similar discrepancy.

Several of the regression models we considered in trying to understand this discrepancy are summarized in Table 1. Model 1 assumes that the SOHFI and bulk measurements differ by a simple factor, which can be interpreted as a calibration adjustment factor for the SOHFI or an overall adjustment of the bulk aerodynamic calculations. However, the radiation term does not depend on wind speed, and thus should not need such an adjustment. Models 3 and 4 account for this fact by separating the turbulent transfer terms from the radiation term. But these models yield a slightly worse fit, weakly favoring a SOHFI calibration error over a turbulent transfer estimation error. On the other hand, model 2, which allows for an offset, fits almost as well as model 1, without requiring a significant adjustment of either the bulk estimate or the SOHFI calibration. Because all known environmental effects on the SOHFI sensors tend to reduce responsivity, the only plausible way the responsivity could be this high is by means of an electronics calibration error. Unfortunately, the necessary instrumentation is no longer available for resolving this issue by remeasurement.

4) Combined day and night results

As noted earlier and explained in Part I, even though the flux sensor used for the Sparkling Lake tests had an aluminized Mylar covering, it still produced a significant spurious response to direct solar irradiance. This can be seen in Fig. 4a, where the daytime SOHFI results show a significant diurnal flux depression that is in phase with the solar flux variation (see Fig. 2c). Given measurements of the solar flux, in this case from the nearby airport, and a calibrated value for the SOHFI solar responsivity, we can largely correct for the spurious solar response. Lacking a laboratory value for the solar responsivity of this sensor, we obtained one from linear regression. The best fit of $H_{\mathrm{SOHFI}} + bH_{\mathrm{Sun}}$ to H_T is obtained with $b = 0.146 \pm 0.010$, providing an rms deviation of 64.7 W m^{-2} between these two curves. The larger scatter in the daytime results partly comes from differences in cloud modulations between the airport and the Sparkling Lake site. The corresponding correlation plot for this model (Fig. 4b) shows the same character that was seen for the nighttime comparisons. Clearly a better fit can be obtained by adjusting the SOHFI calibration or by increasing the convective transfer coefficients. Fit parameters and fit quality for these options are presented in Table 2. The best fit is again for a model in which the SOHFI sensor responsivity is reduced (model 2). This time the reduction is by 24% $\pm$ 2%, which agrees with the nighttime best-fit value of 23% $\pm$ 3% ($=1 - 1/1.3$), well within the uncertainty estimates. Figure 5 displays the fit for this model. The comparison with the bulk calculation is also shown in the correlation plot of Fig. 5b. In spite of the large scatter of the observations, most of which is associated with short-term variations, the overall agreement shows that SOHFI did a reasonable job of tracking the heat flux variations.

To deal with solar influence corrections under conditions for which supporting solar flux measurements are not available, we implemented two design modifi-

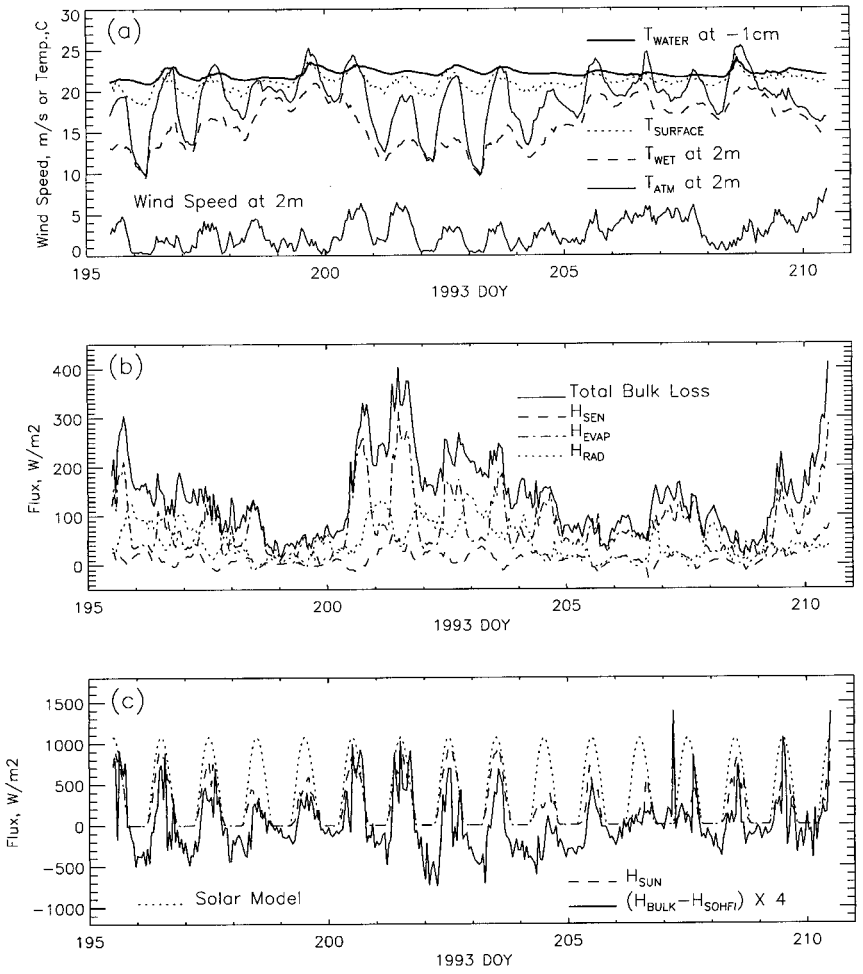

FIG. 2. Sparkling Lake field test conditions: (a) temperatures and wind speed; (b) bulk aerodynamic heat flux components; (c) solar radiation flux estimates compared to $H_{SOHFI} - H_{BULK}$, scaled by an arbitrary factor of 4. DOY = yearday.

cations, as described in Part I: 1) reducing the flux plate sensitivity to solar radiation by using a transparent substrate; and 2) using a second flux plate of high sensitivity to solar radiation to provide a local basis for residual corrections. The analytical approach for determining both the solar correction and the solar irradiance from such measurements is presented in Part I and applied to field measurements in section 2b.

5) OPERATIONAL RESULTS

Although the sensors appeared to function normally for the first few weeks of the Sparkling Lake deployment, problems eventually developed, including 1) sagging of the fiberglass mesh due to float ring shrinkage, allowing the flux plate to drop below the water surface; 2) fouling of the mesh and sensor by biological contaminants; 3) breaking of thermocouple lead wires; and 4) tearing of the fiberglass mesh. To deal with these problems we revised the design to use a rigid support ring to keep the fiberglass mesh under tension, independent of the float dimensional stability, used coating materials that reduce float shrinkage to an acceptable level, and implemented better strain relief for electrical connections. The mesh tears were not located at any high stress points, suggesting that they were created externally, perhaps by birds. Birds have been identified as a serious problem in subsequent ocean deployments.

The floats retrieved at the end of the test were contaminated with a brown residue of presumed biological origin. Particulate matter blown onto the lake from the surroundings and algae growth are both potential sources. Fortunately, the rate of fouling in the ocean appears to be smaller than we saw at Sparkling Lake. Sensors with different solar absorption properties provide a means to monitor possible long-term contamination. Contaminants that would tend to increase the solar absorption of a reflective or transparent sensor might have a neutral or even slightly negative effect on a darkened sensor. Thus a change in the way the two sensors re-

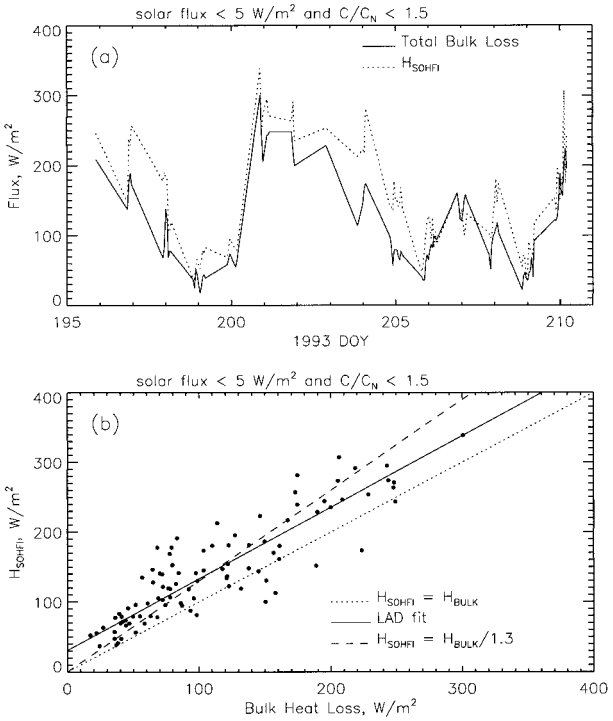

FIG. 3. Sparkling Lake nighttime heat fluxes: (a) SOHFI measurements and bulk aerodynamic estimates as a function of time and (b) correlation plot of SOHFI measurements vs bulk estimates as compared with linear regression lines using least absolute difference (LAD) and to model 1 from Table 1.

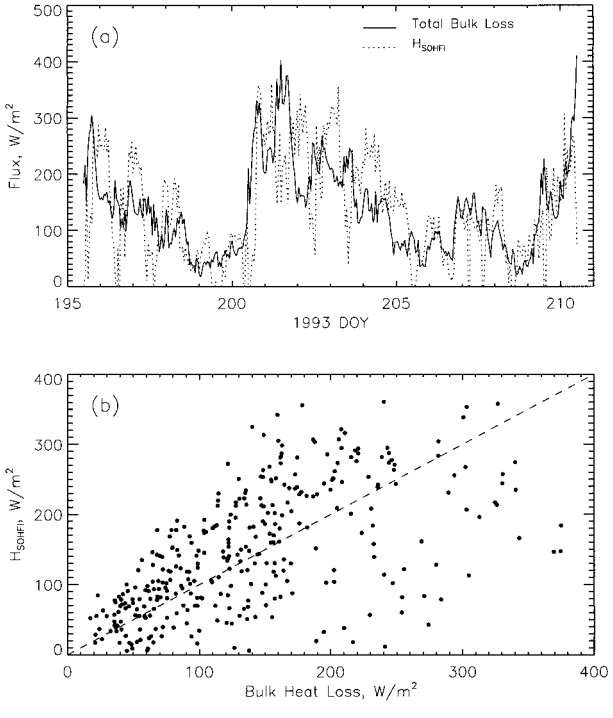

FIG. 4. Sparkling Lake combined day and nighttime heat fluxes: (a) SOHFI measurements and bulk aerodynamic estimates as a function of time and (b) correlation plot of SOHFI measurements vs bulk estimates.

spond to diurnal variations of sunlight can be used to detect and possibly correct for small amounts of contamination.

b. Solar irradiance measurements in Lake Mendota

During 25–28 September 1995, a version of the SOHFI containing both black and clear sensors was deployed on Lake Mendota, a 10 km by 6 km lake of 18–25-m depth, which is adjacent to the University of Wisconsin—Madison campus. Relatively sunny days and light winds provided a good opportunity to test our planned procedure for field calibration of the SOHFI solar responsivity. Independent solar reference measurements were made on the roof of the Space Science and Engineering Center, about 2 mi from the deployed SOHFI, using a LI-COR solar flux sensor, accurate to about 5% according to the manufacturer. The black and clear sensor responses during this period are shown as a time series in Fig. 6. To obtain the excellent nighttime tracking of the two flux sensors required a relative adjustment of 7.2% compared to the nominal calibration value. This differential is very close to the average clear − black difference in manufacturer calibrations for this style of sensors. However, the particular sensors in this instrument had anomalous manufacturer calibrations that have a 4% difference in the opposite direction. The reason for this discrepancy has not been determined. Data during the first half of yearday (JD) 269 were omitted from Fig. 6 because, at that time, the SOHFI drifter was in

TABLE 1. Regression models for Sparkling Lake nighttime observations. Here, H_S and H_E are bulk aerodynamic fluxes, and $H_T = H_S + H_E + H_R$.

Model equation	Coefficient fit values	Rms fit dev (W m^{-2})
(1) $H_{SOHFI} = a_1 H_T$	$a_1 = 1.30 \pm 0.03$	31.0
(2) $H_{SOHFI} = a_0 + a_1 H_T$	$a_0 = 38.4 \pm 6.8$ W m^{-2}; $a_1 = 0.97 \pm 0.05$	33.5
(3) $H_{SOHFI} = a_1(H_S + H_E) + H_R$	$a_1 = 1.327 \pm 0.053$	41.3
(4) $H_{SOHFI} = a_1 H_S + a_2 H_E + H_R$	$a_1 = 1.05 \pm 0.50$; $a_2 = 1.39 \pm 0.12$	41.5

TABLE 2. Regression models for Sparkling Lake combined observations. Here, H_S and H_E are bulk aerodynamic fluxes, and $H_T = H_S + H_E + H_R$.

Model equation	Coefficient fit values	Rms fit dev (W m^{-2})
(1) $H_{SOHFI} + bH_{Sun} = H_T$	$b = 0.146 \pm 0.010$	64.7
(2) $a_1 H_{SOHFI} + bH_{Sun} = H_T$	$a_1 = 0.74 \pm .02$; $b = 0.187 \pm 0.009$	54.3
(3) $H_{SOHFI} + bH_{Sun} = a_1(H_S + H_E) + H_R$	$b = 0.156 \pm .016$; $a_1 = 1.083 \pm 0.049$	72.9

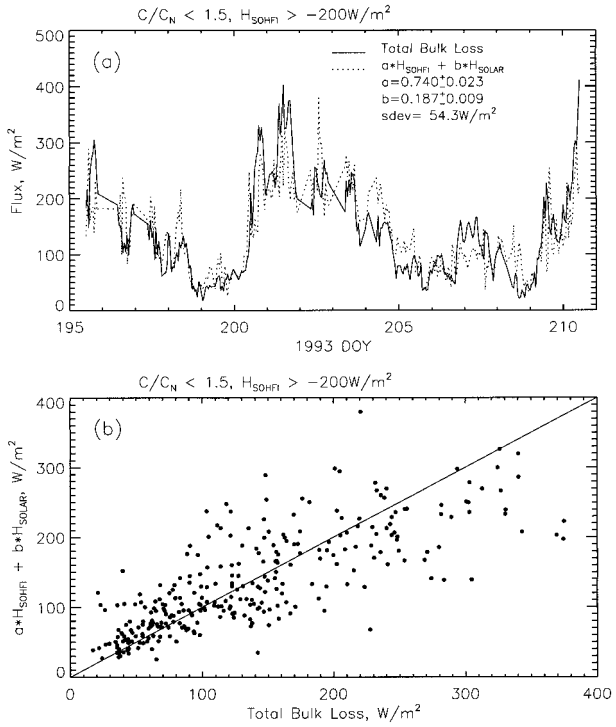

FIG. 5. Sparkling Lake model 2 fit for combined day and nighttime heat fluxes: (a) time series of total heat loss from bulk method (solid line) and corrected SOHFI measurements (dotted line), filtered to reduce the size of diabatic corrections needed and to avoid a few bad data points; and (b) correlation plot of corrected SOHFI measurements vs bulk estimates, compared to the model (line).

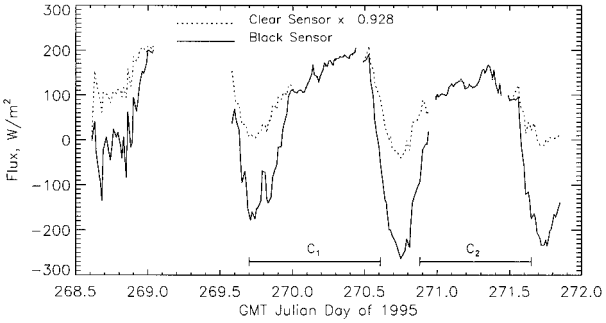

FIG. 6. SOHFI flux measurements on Lake Mendota during predominantly clear weather.

close proximity to the shoreline, and plant material covered portions of the sensors, invalidating the data. The entire system was redeployed to the center of the lake the next morning at JD 269.6.

In Part I, clear and black sensor upward heat flux readings, $H_{\rm clr}$ and $H_{\rm blk}$, are written as

$$H_{\rm clr} = H - k_c H_{\rm Sun} \quad \text{and} \tag{12}$$

$$H_{\rm blk} = H - k_b H_{\rm Sun}, \tag{13}$$

where H is the true upward heat flux, $H_{\rm Sun}$ the downward net solar flux, and $k_c \approx 0.2$ and $k_b \approx 0.5$ are solar response constants that must be determined by calibration. Writing the unknowns as a function of the SOHFI measurements, we obtain

$$H_{\rm Sun} = \frac{(H_{\rm clr} - H_{\rm blk})}{(k_b - k_c)} \quad \text{and} \tag{14}$$

$$H = \frac{[H_{\rm clr} - (k_c/k_b)H_{\rm blk}]}{(1 - k_c/k_b)}. \tag{15}$$

Note that the derived value for the true heat flux depends only on the ratio of k_c to k_b, and not on their absolute values.

Figure 7 displays two solar references we used in the responsivity calibration: the LI-COR solar flux measurements and a geometric clear-sky solar model. The clear-sky model assumes a top-of-atmosphere solar irradiance of 1400 W m^{-2} and a spectrally flat optical depth of 0.15. The periods of close agreement between these two references indicate clear-sky conditions. The third curve in Fig. 7 is a scaled version of $H_{\rm clr} - H_{\rm blk}$, with a scaling factor of 0.29 derived from a fit of $H_{\rm clr} - H_{\rm blk}$ to the $H_{\rm Sun}$, using the solar model as the reference. The fit, shown in Fig. 8, is obtained from what appear to be relatively clear (or dark) periods, labeled as C_1 and C_2 in Fig. 6. According to Eq. (14) the scaling factor is just $(k_b - k_c)$, which has the best-fit value of 0.29 $\pm$ 0.01, implying a solar flux measurement uncertainty of the order of 3%–4%, just due to calibration. However, differences relative to solar reference measurements indicate deviations of 10–20 W m^{-2} at times when cloudiness differences do not appear to be present. We know much less about the response of this system to diffuse sky radiance. It remains to be determined whether its different spectral content may lead to a somewhat different responsivity. Fortunately, the uncertainty due to spectral differences is somewhat ameliorated by the much smaller flux levels associated with diffuse radiation. The diffuse contribution from a clear sky is less than 10% of the direct beam, and a 10% error in measuring the diffuse component then yields an error of 1% of the direct beam, or 14 W m^{-2}. Under moderate cloud cover, say optical depth 2.3 or greater, the diffuse contribution would be even less.

The response ratio k_c/k_b was determined from the cloud-contaminated observations during JD 268. We first computed the relative deviations of points from the average of its nearest neighbors, that is,

$$\Delta H(t_i) = \frac{H(t_i) - [H(t_{i-1}) + H(t_{i+1})]}{2}, \tag{16}$$

where H here stands for $H_{\rm blk}$ or $H_{\rm clr}$ and t_i is the ith sample time. As shown in Fig. 9a, $\Delta H_{\rm blk}$ has nearly twice the response of $\Delta H_{\rm clr}$ to cloud modulations. The correlation plot of $\Delta H_{\rm clr}$ against $\Delta H_{\rm blk}$ from JD 268.65 to JD 269.0 demonstrates a reasonably linear relationship (Fig. 9b). The linear best-fit slope provides the estimate $k_c/k_b = 0.444 \pm 0.006$. Thus the solutions for the dif-

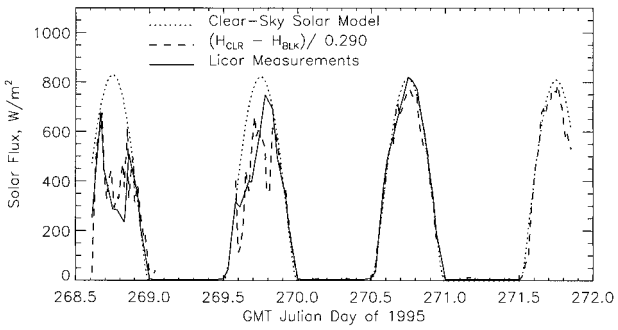

FIG. 7. SOHFI differential flux measurements scaled to match two solar flux estimators, a (LI-COR) solar measurement 2 mi away from the lake and a calculated flux model described in the text. Large sharp variations due to clouds occur at different times for SOHFI and LI-COR measurements.

ference, ratio, and derived absolute values of solar response can be summarized as follows:

$$d = k_b - k_c = 0.29 \pm 0.01(3.4\%), \quad (17)$$

$$r = k_c/k_b = 0.444 \pm 0.006(1.35\%), \quad (18)$$

$$k_b = 0.522 \pm 0.019(3.6\%), \quad \text{and} \quad (19)$$

$$k_c = 0.232 \pm 0.010(4.3\%). \quad (20)$$

The error in the correction of the daytime clear sensor readings is dependent on the error in the ratio r, and on the error in the $H_{\text{clr}} - H_{\text{blk}}$ measurement, but not on the uncertainty in d. If only the uncertainty in the ratio is considered, the fractional error in the corrected flux is just $\sigma_r[r(1 - r)]$, which evaluates to 2.4% of the correction.

3. Open ocean field tests

The SOHFI was exposed to the open ocean environment during field tests in three different locations: the Gulf Stream, the western Pacific near Manus Island, and the Greenland Sea.

a. Gulf Stream deployments

These first SOHFI ocean deployments were conducted mainly to see if the instrument package could survive open ocean conditions; our secondary objective was to obtain meaningful flux measurements under a variety of weather conditions that could be compared with model results or moored buoy data.

1) OPERATIONAL RESULTS

The geographic tracks of the two Gulf Stream deployments are provided in Fig. 10. The first SOHFI drifter package used a 10-in. sensor float and the clear − black configuration with 80-junction thermopiles and wire lead connections. We deployed it on 19 May 1995 (JD 139) about 30 mi east of Miami, Florida. It then

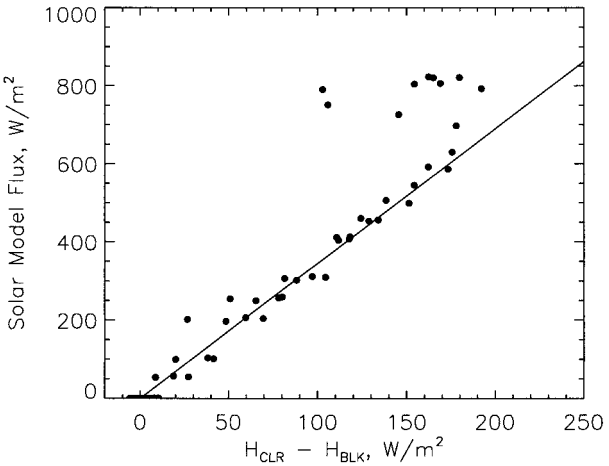

FIG. 8. Solar correlation plot showing the solar model values as a function of the SOHFI-adjusted clear − black difference, for data during clear or dark periods C_1 and C_2 as shown in Fig. 6. The best-fit model (solid line) has a slope of 0.29 ± 0.01.

followed the Gulf Stream north at about 2 kt and eastward at about 0.5 kt, until it got caught in a gyre north of the Bahamas, where we recovered it on 1 June 1995 (JD 152) 60 mi north of Walker's Cay.

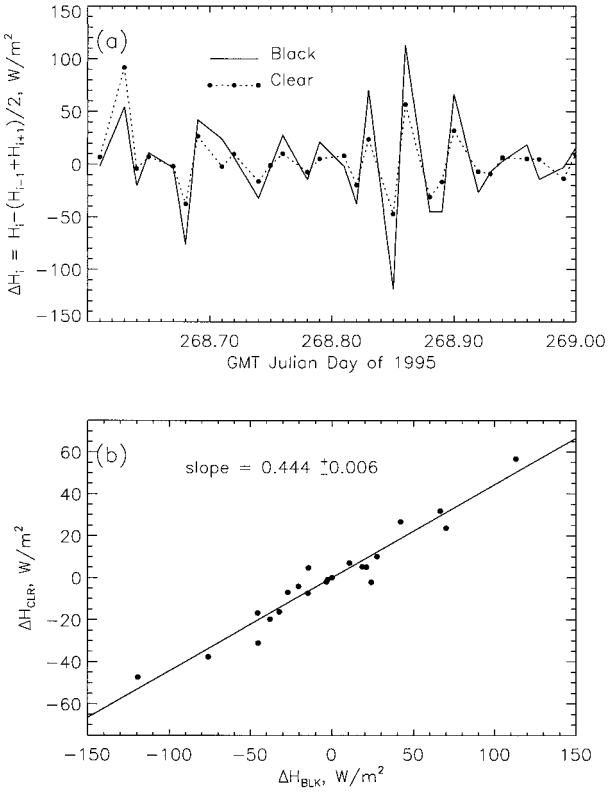

FIG. 9. (a) Clear and black sensor modulation time series and (b) correlation plot that excludes points with $\Delta H_{\text{BLK}} > \Delta H_{\text{CLR}}$. Cloud modulations provide a field method of determining the ratio of clear and black sensor responses to sunlight.

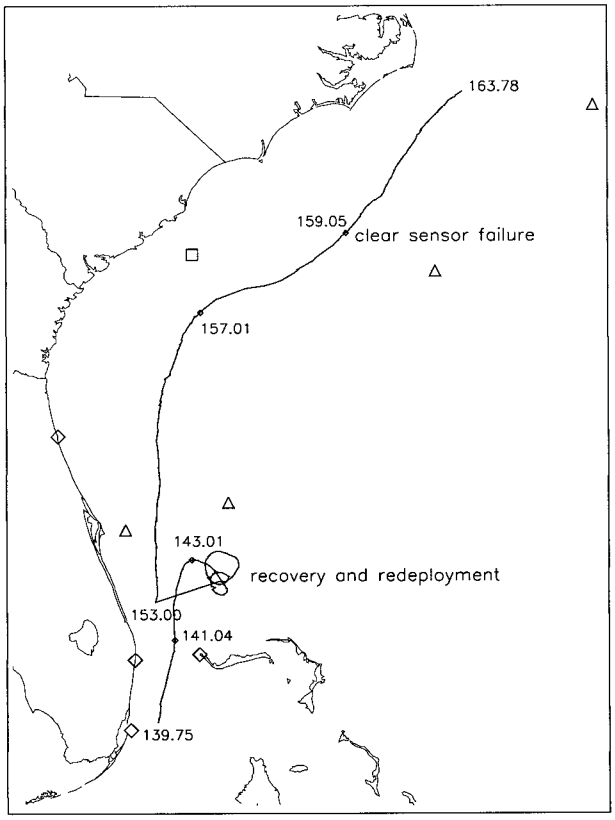

FIG. 10. SOHFI drifter tracks off the southeastern coast of the United States during 19 May–13 June 1995. Points along the drifter track are labeled by yearday. Diamonds mark the locations of C-MAN fixed tower stations; triangles, the 6-m NOMAD moored buoys; and squares, the 3-m discus buoys.

The time series of the flux readings during this interval (Fig. 11a) show that the clear and black sensors were in excellent agreement for periods when valid nighttime data were returned, mostly at the start of day 142. Gaps in valid data occurred for both sensors because the data system software on this first deployment did not correct for the unexpectedly frequent sign flips that occurred within the 20-min averaging periods, a deficiency that was corrected in the second deployment. In addition, the black heat flux sensor became intermittent on day 142 and failed completely on day 143. At recovery we found substantial physical damage to both the foam ring float structure and to the fiberglass mesh, especially in the vicinity of the failed black heat flux sensor. In the opinion of biologists who viewed the damage, it appears to have been caused primarily by seabirds. The portion of fiberglass mesh located directly over the black sensor was mostly missing. Although we found a few small barnacles on the foam ring, the flux sensors were free of biological contamination.

On 1 June 1995 (JD 152), we replaced the first sensor float with an 8-in. float (including a new tether), installed modified software to correct for sensor flip-induced polarity reversals prior to averaging, and redeployed the drifter in the Gulf Stream axis 35 mi southeast of Vero Beach, about 50 mi north of the original deployment. This package was recovered 100 mi southeast of Cape Hattaras, North Carolina, on 12 June (JD 163.78). The time series of flux readings for this second interval (Fig. 12a) shows the same good nighttime tracking as for the first deployment. The absence of data gaps is due to the improved software. However, as can be seen from the departure of the clear and black nighttime readings at the beginning of day 159, about 1 week after deployment, the clear heat flux sensor experienced some sort of failure—its readings dropped to near zero and became noisy. However, the black heat flux sensor continued to function normally throughout the deployment. After recovery on 12 June 1995, we found even more significant physical damage than for the first deployment. Large chunks seemed to have been bitten off the foam float and the clear flux sensor was found completely separated from the supporting mesh, explaining its anomalous response characteristics. Again the damage appeared to be caused by seabirds.

Both drifter buoys and sensor float rings were painted white, and probably were quite visible to seabirds flying overhead. In spite of their visibility and location in regions of high seabird populations, the sensors still functioned normally for up to a week. Options for reducing damage from seabird attacks include camouflage, more rugged construction methods, and bird-repelling spines. Our latest design, the Greenland Sea version described in Part I, uses more rugged ribbon leads and much tougher foam to protect against damage even if the floats are spotted by birds.

2) SOLAR FLUX COMPARISONS

Because flux data from the first deployment were not corrected for flip-induced sign reversals prior to averaging, and because of early failure of the black sensor, there is very little useful solar response information that can be gleaned from this first period. Figure 11 does show that the black heat flux sensor reading is depressed by incident sunlight about twice as much as the clear sensor, and the limited data in Fig. 11c show that the scaled clear − black difference is roughly consistent with the local solar flux, in the sense that the peak values fall within the envelope provided by the geometric solar model (we used an effective optical depth of 0.15 here, although that is not well constrained by the observations).

Solar flux information from the second period is shown in Fig. 12b, where the expected clear-sky solar flux is compared to the inferred value of $(H_{\mathrm{clr}} - H_{\mathrm{blk}})/0.29$, obtained from Eqs. (14) and (17). Among the first six days of this deployment, when both clear and black sensors were functioning normally, only the last seems relatively free of heavy cloudiness. But even that day is not as clear as we assumed for the model calculations. Two measurements confirm that the day 153–159 period

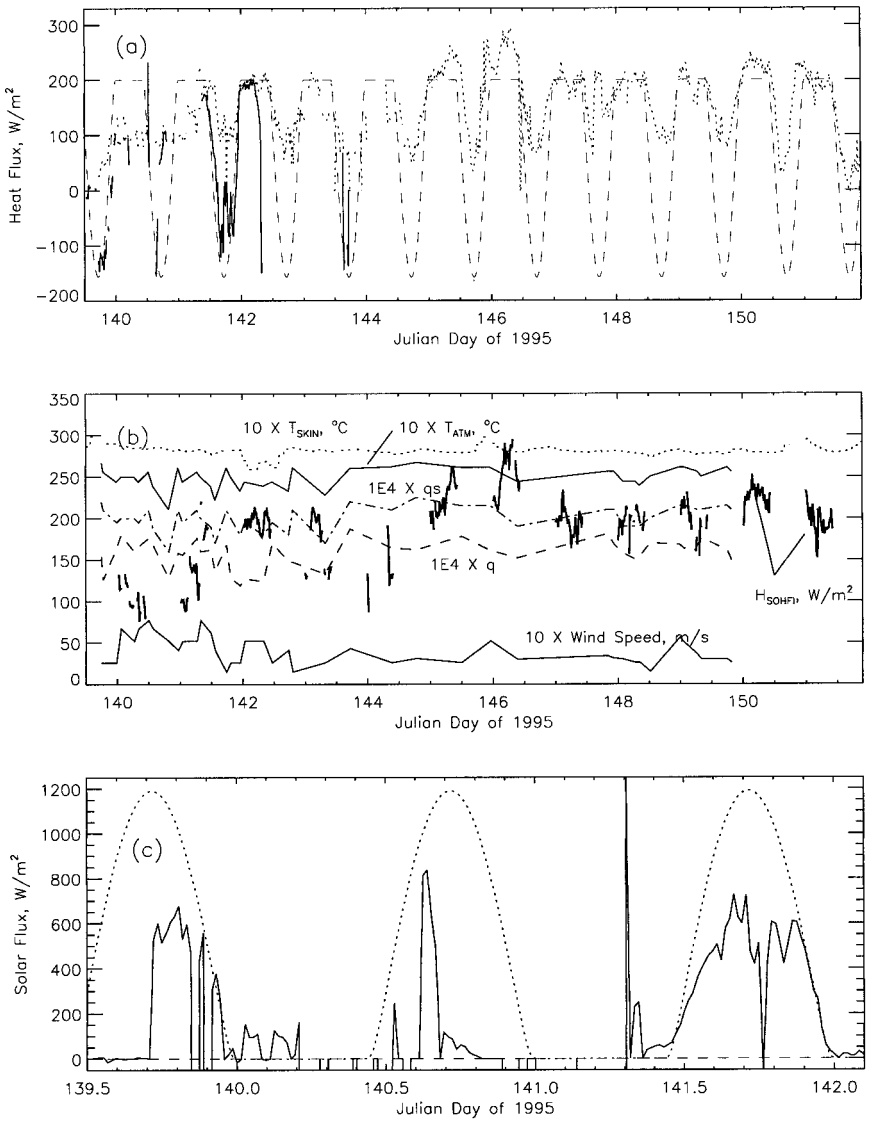

FIG. 11. Results from the first phase of the Gulf Stream deployments: (a) SOHFI flux measurements by clear sensor (dotted) and black sensor (solid); (b) nighttime clear sensor readings and nearby moored buoy observations of wind, temperature, and humidity; (c) solar flux estimates from clear − black differences, compared to solar model estimates (dotted line). The black sensor became intermittent early and failed completely on day 143.

was at no time completely clear: 1) the diurnal variation of H_{blk} is notably larger two days later, and 2) skin temperature measurements show stronger diurnal variations two days later.

3) HEAT LOSS COMPARISONS

Weather conditions during the two SOHFI deployments ranged from sunny and clear, to thunderstorms and the decaying stage of Tropical Storm Allison. Observations from moored buoys and fixed towers (locations shown in Fig. 10) provide comparison data.

First deployment. The nighttime flux values for both clear and black detectors were in approximate agreement prior to the failure of the black sensor near JD 143.9, including the increase from about 100 W m^{-2} to nearly 200 W m^{-2} during yearday 141.1–141.4 (Fig. 11a). On day 140, average wind speeds were greater than 5 m s^{-1} and less than 8 m s^{-1}, as indicated from nearby moored buoys. This was also a day on which thunderstorm and rain shower activity occurred in the vicinity of the SOHFI, as indicated by radar summaries. The lack of solar depression in the daytime flux readings confirms the generally persistent cloud cover. Measured heat fluxes on this day were a relatively modest 100 W m^{-2} but increased by a factor of 2 after the weather

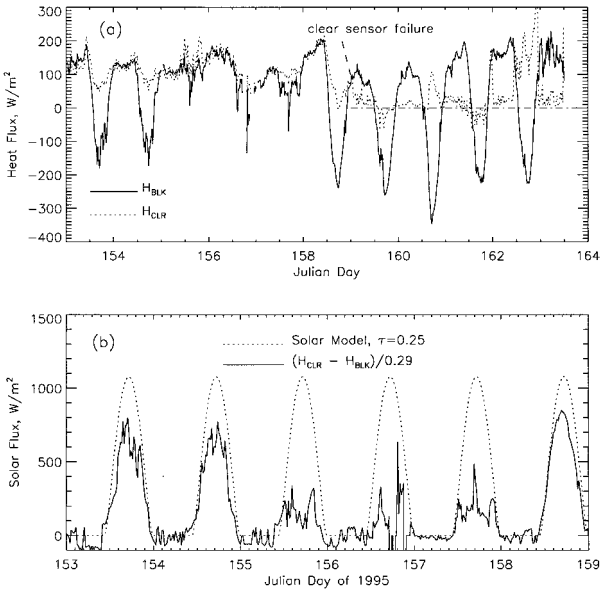

FIG. 12. SOHFI clear and black sensor flux readings during the second phase of the 1995 Gulf Stream deployment: (a) time series and (b) solar flux estimate based on clear − black difference flux, compared to a solar model flux calculation with vertical optical depth 0.25. Prior to the clear sensor failure at the start of day 159, the two sensors provided consistent nighttime readings.

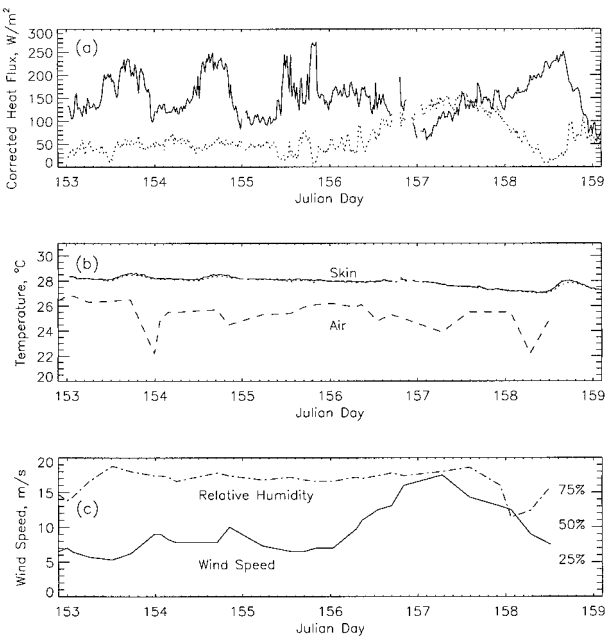

FIG. 13. Results during the passage of Tropical Storm Allison: (a) total corrected heat flux (solid line) and 3 × submergence percentage (dotted line), (b) atmospheric and skin temperatures for clear sensor (dotted line) and black sensor (solid line), and (c) humidity and wind conditions during the passage of Allison. In (a) the peak of the submergence curve is at about 50%.

cleared in the middle of day 141. Examination of nearby buoy observations shown in Fig. 11b does not provide an obvious explanation for the change. However, the sudden increase during the night of JD 141 is compatible with the clearing of cloud cover and increased radiation losses. Heat losses were near 200 W m^{-2} over most of the remaining period, with the notable exception of days 145 and 146, when they reached nearly 300 W m^{-2}. The origin of this increase cannot be explained by significant changes in any of the factors affecting turbulent transport: wind speed, air temperature, and humidity exhibited only small variations. One possible explanation is that conditions at the SOHFI during this period were not well represented by the observations made at the relatively distant moored buoys (see Fig. 10). Another possibility is that clearing of aerosols allowed more net thermal radiative heat loss during this period. Unfortunately, there are no ancillary measurements that can test this hypothesis. Sensor problems are not a likely explanation for the high flux values for two reasons: 1) the clear sensor was found to be undamaged when recovered, and 2) virtually all conceivable sensor problems would lead to reductions in the measured fluxes.

Second deployment. The second period of observations, beginning on day 153, provided six nights during which clear and black sensors should have provided the same readings, and this expectation was met, but only approximately. Over this period, the sensors had a peak difference of about 30 W m^{-2}, and an rms difference of about 10 W m^{-2}. But during the first half of day 157 the differences were well below these levels. The time variation of this difference can be obtained from Fig. 12b by multiplying the nighttime solar flux estimator by a factor of 0.29.

An interesting event during the second 1995 Gulf Stream deployment was the passage of the remnants of Tropical Storm Allison (Pasch 1996). Winds during this time period rose from 6 m s^{-1} to a sustained high of 14 m s^{-1} as the eastern fringe of Allison intersected the route taken by the SOHFI drifter. Allison passed over the drifter position during days 157 and 158 with peak wind speeds of 17.5 m s^{-1} measured at a nearby National Data Buoy Center discus buoy (see Fig. 10). The SOHFI heat flux and skin temperature measurements are presented in Fig. 13, along with the buoy wind speed measurements. The clear and black heat flux sensors agreed well during this period for which the absorbed solar radiation was minimal because of extensive cloud cover. Relative to conditions on day 156, the air became colder and the wind speed increased by nearly a factor of three, while the humidity stayed near 75%. These changes should have increased the turbulent transports dramatically. Using Fig. 1c as a guide, we might have expected increases of at least several hundred watts per square meter. Instead, the measured heat flux actually *decreased* by about 100 W m^{-2}, suggesting that, for this early season storm, the observed decrease in ocean surface temperature might be due more to increased ocean mixing rather than surface heat losses.

A more probable alternative explanation for the low

heat fluxes that were measured during high wind periods is that the SOHFI sensor responsivity decreased as a result of the heavy weather, either because of fundamental limitations related to the sensor's interaction with the water surface, of the type found in laboratory measurements at much higher flux levels (Part I), or because the submergence filtering was not effective. The latter possibility is suggested by the lack of any significant difference between submergence-filtered and unfiltered data, in spite of the significantly increased submergence counts during the period of anomalous flux decrease (see Fig. 13a). This can be understood if the actual flux sensor submergences are not well correlated with the submergences detected at the edge of the float, and thus do not get filtered out of the averages. In a Pacific deployment, discussed later, a different configuration of submergence pins, placing them much closer to the flux sensors, did show a distinct difference between submergence-filtered and unfiltered observations, by as much as 40–50 W m^{-2}. Thus, it seems likely that the Gulf Stream flux measurements during high winds are low at least partly because of poor submergence filtering.

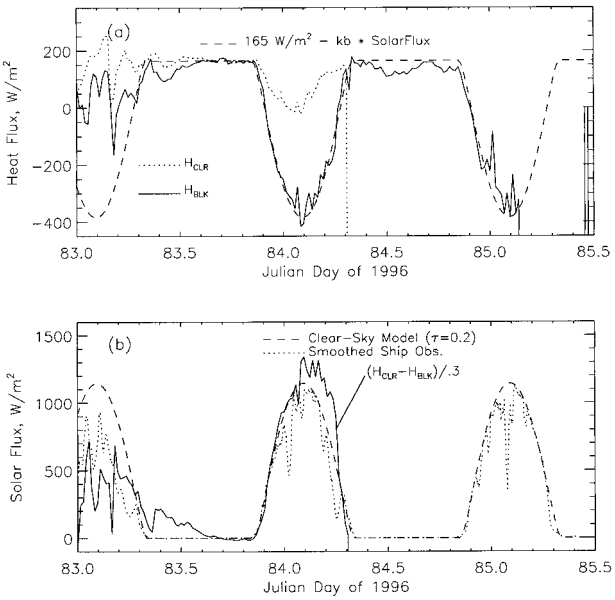

FIG. 14. SOHFI results during Combined Sensor Program cruise: (a) clear and black flux measurements and (b) solar flux estimates from clear − black differences.

4) SKIN TEMPERATURE MEASUREMENTS

The clear and black SOHFI flux sensors each have an embedded thermocouple for measuring skin temperature (see Part I). During the Gulf Stream deployment the difference in the two skin temperature measurements, $T_{\text{black}} - T_{\text{clear}}$, was $\approx 1.5 \times 10^{-4}$ °C (W m^{-2})$^{-1}$ of downward solar flux, and, during a clear day, the diurnal variation in this difference was about 0.18 K. The clear thermocouple registered its own diurnal variation of about 0.4 K, about 0.14 K of which was due to absorption associated with the flux plate, and the remaining 0.26 K (about ⅔ of the direct response) representing true surface temperature variation. This partitioning assumes that the solar heating reponse ratio for the clear and black sensors is proportional to their solar flux responsivity ratio. This diurnal variation is far below the 3 K seen in the Combined Sensor Program (CSP) deployment (discussed in the next section), but fairly typical for light to medium wind conditions (Price et a1. 1986).

b. The western Pacific deployment

A modified engineering model SOHFI drifter took part in the CSP cruise of 1996 (Post et al. 1997). The purpose of CSP was to understand relationships between atmospheric and oceanic variables that affect radiative balance in the warm pool of the Pacific, a region that plays a significant role in El Niño and the Southern Oscillation. A wide variety of in situ and remote instruments were assembled to make measurements in support of that goal. Many of the instruments were aboard the National Oceanic and Atmospheric Administration's (NOAA's) R/V *Discoverer*, including the SOHFI, which was deployed from a station-keeping position 100 n mi off Manus Island. In this engineering model configuration of SOHFI, submergence pins were positioned directly between the clear and black sensors. Our primary objective in participating in the cruise was to carry out intercomparisons between our SOHFI observations and eddy correlation measurements; our secondary objective was to make comparisons with local bulk aerodynamic estimates and model results. We obtained valuable comparisons with the bulk aerodynamic methods, but were unable to compare with eddy flux results, as none were available during the SOHFI deployment.

The SOHFI package entered the ocean on JD 83.167 (0400 UTC 23 March 96), after which the ship maintained position while the drifter was carried along by a strong westward current for a distance of roughly 60 km during the 2-day deployment. Except at the very beginning and end of the deployment, the separation between the ship and the drifter made it difficult to compare SOHFI and shipboard solar observations because of partial cloudiness that introduced strong local variability. Nevertheless, it is obvious that the SOHFI clear sensor experienced problems almost from the moment it entered the water. As shown in Fig. 14, the clear sensor completely failed at JD 84.3, showed poor solar tracking just hours before that, and during the previous night disagreed with the black sensor heat flux by varying amounts. Thus, we consider these clear sensor flux measurements as invalid. On the other hand, the black sensor's excellent tracking of the solar model fluxes

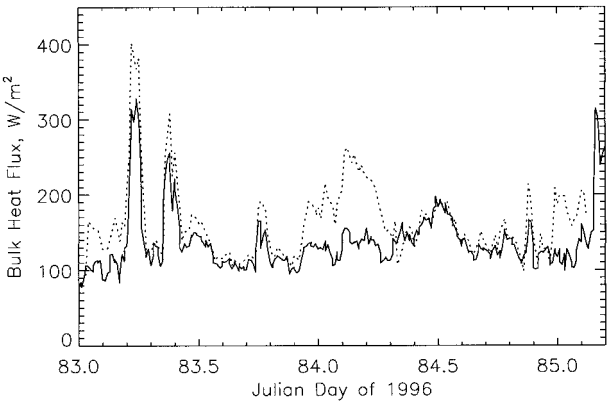

FIG. 15. Comparison of bulk aerodynamic heat flux estimates during the CSP cruise: the Kondo calculation using SOHFI skin temperatures (dashed line), and results from the COARE 2.0 algorithm (Fairall et al. 1996) based on shipboard measurements of surface temperature (solid line).

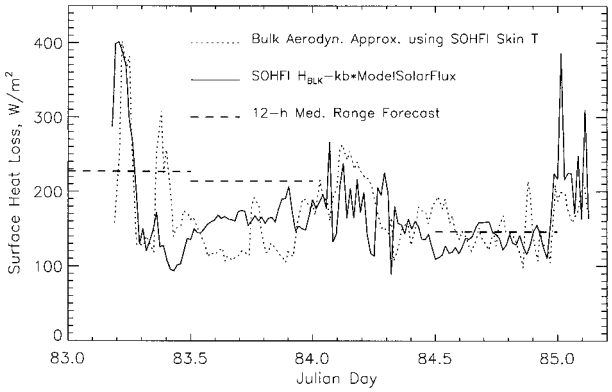

FIG. 16. Comparison of SOHFI and independent heat flux estimates during the CSP deployment.

during days 84 and 85 indicate relatively clear weather as well as stable sensor performance.

Shipboard measurements of winds, air temperature, humidity, and sea surface temperature, and downwelling longwave and solar fluxes, made it possible to carry out a bulk aerodynamic analysis during the CSP deployment, although the bulk estimates were strictly valid only near the ship, and thus of variable relevance to the SOHFI observations. We used these data to compute fluxes using Kondo's method and obtained close agreement with the results of Fairall's Coupled Ocean–Atmosphere Response Experiment 2.0 (COARE 2.0) bulk calculations. (C. W. Fairall 1997, personal communication). The results are shown in Fig. 15. The main discrepancy is seen for the daytime fluxes and is of a magnitude that might be expected from the difference between surface and ship intake temperatures. We used the local skin temperature measured by the SOHFI, and Fairall used the bulk temperature from the ship intake, corrected for cool skin and warm layer effects using an algorithm that takes into account solar and thermal radiative fluxes (Fairall et al. 1996).

SOHFI measured a surprisingly large 3°C diurnal variation in skin temperature during a day with wind speeds generally less than 2 m s^{-1}. According to Price et al. (1986), diurnal variations of 2°–3°C can be obtained under summer heating conditions with vanishing winds that allow a trapping depth of thermal response as small as 1 m, but with light to moderate winds, solar heating is distributed over a deeper layer and diurnal variations are typically of the order of 0.2°C, which is comparable to the 0.4°C that we measured during the clear days of the Gulf Stream deployment. The existence of a large diurnal variation during the SOHFI deployment was confirmed by radiometric skin temperature measurements using the shipboard Marine Atmospheric Emitted Radiance Interferometer (AERI) instrument (R. Knuteson 1998, personal communication), although only a 2°C variation was seen in the radiometric data. The daytime heat fluxes obtained using the SOHFI skin temperatures in the bulk aerodynamic calculation are in reasonably good agreement with the measured heat fluxes. They would probably agree slightly better if we had used the AERI skin temperatures. The difference between SOFHI and AERI skin temperature measurements is partly due to anomalous local heating due to the presence of the flux plate, and may also be partly due to a real difference, given that the SOHFI and shipboard measurements were up to 50 km apart during this period.

Because only the black sensor appeared to be functioning consistently, we could not correct for solar perturbations of the black sensor using clear and black measurements in Eq. (15). Instead, we needed to use an independent solar flux estimate to correct the black sensor measurement using Eq. (13). We considered both the shipboard measurements and solar model calculations and decided on the solar model calculations to reduce the cloud-induced noise level. By using shipboard measurements with cloud perturbations that did not match the cloud perturbations at the SOHFI location, we would include both perturbations in the corrected fluxes. On the other hand, by using the model solar fluxes, we see only the cloud perturbations in the SOHFI measurements. The comparison of the black sensor output with the solar model flux indicates that the skies were mainly clear on the second and third days of the deployment. To obtain the corrected surface heat loss, we added $0.48H_{\mathrm{Sun}}$ to H_{blk}.

The solar-corrected SOHFI heat loss measurements are compared with bulk aerodynamic results in Fig. 16. Considering that during most of the time period shown the SOHFI was not very close to the ship, the overall agreement is reasonably good: the average values are close, and the variations are of comparable size. Shortly after deployment both the ship measurements and SOHFI tracked a large pulse in surface heat loss, a result of a pulse of 7.5 m s^{-1} wind speeds over a background level near 1–2 m s^{-1}. The increased winds were accompanied by a drop in air temperature as well. Both effects

TABLE 3. Comparison of average heat fluxes during SOHFI CSP deployment. The first SOHFI average is for the period JD 83.18–83.5.

	Flux estimation method		
Averaging period (JD)	Bulk aerodynamic (W m^{-2})	SOHFI (W m^{-2})	MRF 12-h forecast (W m^{-2})
83–83.5	183 ± 14	192 ± 22	227
83.5–84	137 ± 5	163 ± 2	214
84–84.5	186 ± 7	168 ± 6	
84.5–85	150 ± 5	139 ± 4	146

contributed to the greatly increased heat loss, from about 120 to nearly 400 W m^{-2}. A second pulse, indicated by shipboard observations near JD 83.4, was not seen by the SOHFI flux measurements, probably because SOHFI had already separated from the ship sufficiently that local wind conditions were different.

Also plotted in Fig. 16 are the 12-h forecast results from the Medium-Range Forecast (MRF) model, shown as horizontal bars extending over the periods for which the predicted averages are computed. Parameterizations of the sensible, latent, and radiation heating used in the MRF model yield results comparable to SOHFI measurements and to the bulk aerodynamic calculations. Considering that the MRF calculations are made on 2.5° latitude by 2.5° longitude grids, the agreement between the MRF parameterizations and the local measurements may be as close as can be expected. Twelve-hour averages for all three heat flux estimates are provided in Table 3. The bulk aerodynamic results in this table use the Kondo equations and the SOHFI skin temperature measurements. Uncertainties in the average are formal values derived from the variance of the samples used to compute the average and do not include systematic errors.

During the night of day 83 (JD 83.5–84), the bulk aerodynamic fluxes are significantly lower than the SOHFI measurements. This difference occurs during periods when winds were mainly below 2 m s^{-1}. However, during the night of JD 84, there is a marked improvement between the measurements and the bulk formula calculations. This period was dominated by winds averaging about 3.5 m s^{-1}, and stability conditions closer to near-neutral.

c. The Greenland Sea deployment

During 17–23 May 1997 (JD 137.8–142.8), two complete SOHFI systems were deployed in the Greenland Sea and subsequently recovered. Both used the ruggedized, but low responsivity, sensors and the float design illustrated in Fig. 3c of Part I. The two systems differed only in the color of the Niiler buoy (one was painted gray and the other orange). The gray color was chosen to provide some degree of camouflage in hopes of avoiding bird detection. The orange color used on one drifter was chosen to maximize our chance of recovering it. Unfortunately, the two systems were deployed relatively close together in time and never separated by very much distance, marring the effectiveness of our camouflage test. Both floats were eventually attacked by seabirds, the first evidence being a spike of sustained float submergence 2.6 days after deployment (for the orange system) and 2 days after deployment (for the gray system). These sustained submergence events occurred just after the intense winds and cloudy weather abated (judging from solar flux levels, and overall submergence counts, which dramatically decreased at the end of day 131). At recovery, the drifters were easy to spot because of the birds that were hovering over them. Both floats were found with damaged mesh, although the flux sensors were intact and did not exhibit any electrical problems.

During the first half of the deployment, bird attacks were probably inhibited by the heavy weather. The subfreezing temperatures, 30-kt winds, and 10-m wave heights during the early part of the deployment all presented new challenges to the measurement system. Measured fluxes were quite small throughout the deployed period, ranging from about 30–60 W m^{-2}. During the early high-wind period, signal sign reversals designed to compensate for float orientation reversals, seemed to be associated with unusually high noise levels, especially for the gray drifter where spikes of 10–20 W m^{-2} were common. This noise is a result of preamplifier input offsets, which do not reverse with float orientation reversals. The effect was first noticed in this deployment because the preamp offsets were increased by low operating temperatures (see Part I for an explanation of offset effects and correction methods). Noise levels following this stormy period, when the sensor was not flipping very often, were much smaller for both systems, generally under 1 W m^{-2}, except during periods where bird attacks seemed to be happening.

4. Discussion and conclusions

While the laboratory tests (Part I) showed relatively close agreement (≈10%) between the skin-layer heat flux measurements and independent calorimetric measures, at least up to relatively high flux levels, the results of the field tests so far are not definitive with respect to either the accuracy of the measurement, or the operating limits of the system. Encouraging results from the Sparkling Lake and CSP comparisons still have limitations regarding the relevance of the results to serve as heat flux references. The bulk aerodynamic comparisons seem to be best when the input observations are made in close proximity to the SOHFI, yet we have a very small dataset for which such comparisons are available. And we have so far obtained no coincident comparisons with eddy heat flux observations. Comparisons with solar flux measurements during the Lake Mendota

deployment were also encouraging, but equivalent long-duration comparisons in the open ocean are still needed.

A second key element of field tests in the open ocean is pure survival. Problems with saltwater invasion of connectors and sensors were resolved in the laboratory prior to field tests. Additional design changes were made in the flux sensors to increase ruggedness, mainly to avoid costly patchwork repairs required to carry out laboratory checkouts prior to field deployments. The new sensor design has yet to experience a single saltwater leak problem, even after bird attacks. The remaining major survival problem is finding an effective way to deal with birds. Survival times are limited by the fragility of the fiberglass mesh when exposed to pecking by seabirds. Although the data system and flux sensors continue to function after such attacks, the data are no longer valid because sensors are no longer properly positioned within the conduction layer. We have tested alternative mesh materials of greater ruggedness but have so far found none that do not also perturb the heat flux measurements to an unacceptable degree. We are currently investigating the use of spines that project outward from the float ring and extend above the fiberglass mesh. Such structures are commonly used to deter birds in commercial settings. From limited lab investigations, it appears possible to implement such a countermeasure without significantly altering the flux measurements. The field performance of such a system remains to be determined.

Our analysis of the SOHFI measurements in lake and ocean environments support the following conclusions.

1) Solar irradiance monitoring and field calibration techniques, using a pair of flux sensors with different solar absorption characteristics, were demonstrated by a combination of freshwater and ocean deployments. Tracking of solar irradiance diurnal variations seems to be accurate to within about 5% of maximum values, or better, although further investigation is needed to account for the effects of changing spectral distributions of sunlight.
2) Preliminary field tests of SOHFI have shown reasonably close agreement with bulk aerodynamic heat flux estimates in freshwater and ocean environments (generally within about 20%), although there is a possible systematic error of 20%–30% in the freshwater comparisons at Sparkling Lake. The best tracking of flux variations has occurred when both SOHFI and independent observations are in close proximity, conditions that have rarely been achieved in ocean deployments to date.
3) Depressed flux levels during storm passages may be mainly due to a fundamental limitation in performance under high wind conditions, but at least part of the depression is caused by poor submergence filtering for early sensor designs that used submergence pins on the float ring. Placing submergence pins in the direct vicinity of the flux sensors is a promising way to minimize this problem.
4) SOHFI deployments in the Gulf Stream, in the western Pacific, and the Greenland Sea, demonstrated functionality of sensors and the data system in an ocean environment. However, seabird attacks have provided a significant impediment to long-term (several months) survival and pointed out the need for design modifications to evade detection by birds, to prevent attacks when detected, and to improve resistance to attacks.
5) Better estimates of performance and limitations of this device require good intercomparison tests under field conditions. While the results so far have been encouraging, the precise accuracy of the SOHFI sensor measurements under field conditions is still not established. We need extended intercomparisons with independent techniques, preferably eddy-correlation measurements.

Acknowledgments. This research was partially supported by NSF Grants ATM-9419535 and ATM-92216065 through the NSF Physical Meteorology Program, directed by Ronald Taylor of NSF, and by the University of Wisconsin Space Science and Engineering Center (SSEC); Francis Bretherton, director; and Robert Fox, executive director. We thank Gene Bucholtz, Nikola Ciganovich, Mike Dean, Pat Fry, Robert Herbsleb, Robert Knuteson, Ronald Koch, Dennis McRae, Mark Mulligan, Robert Paulos, Henry Revercomb, Evan Richards, John Short, Jerry Sitzman, and Paul Wisniewski from SSEC, who contributed to the design, development, and field deployment efforts. We thank Barbara Benson and Tim Kratz of the University of Wisconsin Limnology Center for providing correlative data supporting the Sparkling Lake deployment. We thank Kim Van Scoy of the University of Wisconsin Department of Atmospheric and Oceanic Sciences for conducting the Greenland Sea deployment and recovery. We thank Scott Craven of the University of Wisconsin Department of Wildlife Ecology for advising on bird countermeasures and Glen Lee of the University of Wisconsin Limnology Laboratory for assisting with Lake Mendota deployments. We thank M. J. Post, the CSP mission scientist; and Chris Fairall of NOAA/ETL/ERL, Boulder, Colorado, who provided CSP comparison data. We thank Sharyn Chester of NOAA/NMFS, Beaufort, North Carolina, who evaluated the biological damage evidence. We thank Christopher Moore and Larry Kanitz of University of Miami Rosential School of Marine and Atmospheric Science for assisting with two Gulf Stream deployments and one recovery. We thank Captain Ogus and the crew of the R/V *Cape Hatteras* for efforts in carrying out the second Gulf Stream recovery.

REFERENCES

Bradley, E. F., P. A. Coppin, and J. S. Godfrey, 1991: Measurements of sensible and latent heat flux in the western equatorial Pacific Ocean. *J. Geophys. Res.,* **96** (Suppl.), 3375–3389.

Fairall, C. W., E. F. Bradley, D. P. Rogers, J. B. Edson, and G. S. Young, 1996: Bulk parameterization of air–sea fluxes for Tropical Ocean Global Atmosphere Coupled-Ocean Atmosphere Response Experiment. *J. Geophys. Res.*, **101** (C2), 3747–3764.

Fleagle, R. G., and J. A. Businger, 1980: *An Introduction to Atmospheric Physics.* Academic Press, 432 pp.

Guymer, T. H., J. A. Businger, K. B. Katsaros, W. J. Shaw, P. K. Taylor, W. G. Large, and R. E. Payne, 1983: Transfer processes at the air–sea interface. *Philos. Trans. Roy. Soc. London,* **A308,** 253–273.

Kondo, J., 1975: Air–sea bulk transfer coefficents in diabatic conditions. *Bound.-Layer Meteor.,* **9,** 91–112.

Kraus, E. B., 1972: *Atmosphere–Ocean Interaction.* Oxford University Press, 275 pp.

List, R. J., 1963: *Smithsonian Meteorological Tables.* Smithsonian Institution, 527 pp.

Pasch, R. J., 1996: Preliminary report of Hurricane Allison, June 3–6. [Available online at http://www.nhc.noaa.gov/1995allison.html.]

Post, M. J., and Coauthors, 1997: The Combined Sensor Program: An air–sea science mission in the central and western Pacific Ocean. *Bull. Amer. Meteor. Soc.,* **78,** 2797–2815.

Price, J. F., R. A. Weller, and R. Pinkel, 1986: Diurnal cycling: Observations and models of the upper ocean response to diurnal heating, cooling, and wind mixing. *J. Geophys. Res.*, **91,** 8411–8427.

Rao, K. S., J. C. Wyngaard, and O. R. Cote, 1974: The structure of the two-dimensional internal boundary layer over a sudden change of surface roughness. *J. Atmos. Sci.,* **31,** 738–747.

Sromovsky, L. A., J. R. Anderson, F. A. Best, J. P. Boyle, C. A. Sisko, and V. E. Suomi, 1999: The Skin-Layer Ocean Heat Flux Instrument. (SOHFI). Part I: Design and laboratory characterization. *J. Atmos. Oceanic Technol.,* **16,** 1224–1238.

Stull, R. B., 1988: *An Introduction to Boundary Layer Meteorology.* Kluwer Academic Publishers, 666 pp.

Suomi, V. E., L. A. Sromovsky, and J. R. Anderson, 1996: Measuring ocean–atmosphere heat flux with a new in-situ sensor. Preprints, *Eighth Conf. on Air–Sea Interaction and Conf. on the Global Ocean-Atmosphere-Land System (GOALS)*, Atlanta, GA, Amer. Meteor. Soc., 38–42.